energies

MDPI

Article

Control Comparison for the Coordinate Transformation of an Asymmetric Dual Three Phase Synchronous Motor in Healthy and Single-Phase Open Fault States

Dong-Kyun Son, Soon-Ho Kwon, Dong-Ok Kim, Hee-Sue Song and Geun-Ho Lee *

Electric Motor Control Laboratory, Graduate School of Automotive Engineering, Kookmin University, Seoul 02707, Korea; dkson92@kookmin.ac.kr (D.-K.S.); qwer727@kookmin.ac.kr (S.-H.K.); a2016007@kookmin.ac.kr (D.-O.K.); metamong@kookmin.ac.kr (H.-S.S.)
* Correspondence: motor@kookmin.ac.kr

Abstract: The coordinate transformation method of asymmetric dual three phase synchronous motor (ADTP-SM) is a Double dq transform using two *dq*-axes and a vector space decomposition (VSD) model method using the orthogonality of ADTP-SM. There are several studies comparing the two methods in a healthy state, but few in a single-phase open fault state. In the healthy, when the VSD model is applied, different harmonic orders of the phase current are projected onto the *dq* and *xy*-axes (the axis for controlling harmonics of the phase current), and the two-axes are orthogonal, so it can be controlled stably. In the single-phase open fault state, the same current control logic as in the healthy situation is applied. When applying the Double dq transform, the *dq*-axis of the fault set fluctuates, and it affects the healthy set, so it cannot be controlled stably. When applying the VSD model, if both the *dq*-axis and the *xy*-axis are controlled, the two coordinate systems do not have orthogonality and cannot be stably controlled, due to mutual interference. However, if only the *dq*-axis is controlled, it can be controlled stably because there is no Cartesian coordinate system other than the *dq*-axis. In the healthy state and single-phase open fault state, the equation is verified through experiments and simulations, and the control stability according to the coordinate transformation is compared.

Keywords: asymmetric dual three phase synchronous motor; vector space decomposition; double dq transform; magneto motive force

check for updates

Citation: Son, D.-K.; Kwon, S.-H.; Kim, D.-O.; Song, H.-S.; Lee, G.-H. Control Comparison for the Coordinate Transformation of an Asymmetric Dual Three Phase Synchronous Motor in Healthy and Single-Phase Open Fault States. *Energies* **2021**, *14*, 1735. https://doi.org/10.3390/en14061735

Academic Editor: Rukmi Dutta

Received: 16 February 2021
Accepted: 16 March 2021
Published: 21 March 2021

Publisher's Note: MDPI stays neutral with regard to jurisdictional claims in published maps and institutional affiliations.

Copyright: © 2021 by the authors. Licensee MDPI, Basel, Switzerland. This article is an open access article distributed under the terms and conditions of the Creative Commons Attribution (CC BY) license (https://creativecommons.org/licenses/by/4.0/).

1. Introduction

An asymmetric dual three phase synchronous motor (ADTP-SM) is a motor with high torque density and high reliability. It is primarily used for hybrid starter generator (HSG) motors for automobiles and traction motors for elevators and ships [1–3]. The motor has two sets of three-phase windings that are out of phase by 120 degrees. This paper describes a motor in which two sets are phase-shifted by 30 degrees of an electrical angle with isolated neutral points, as shown in Figure 1 [2]. This can improve the electrical performance by increasing the winding-coefficient and increasing the torque ripple order compared to the conventional three-phase motor [1–4]. It is regarded as two independent three-phase motors having a phase difference of 30 degrees from each other, and many studies have been conducted for control using two sets of voltage source inverters [5,6]. However, it is not mechanically separated but electrically coupled. This means that the larger the mutual inductance between each set, the stronger the magnetic coupling and the control characteristics may be adversely affected. Much research is being conducted to improve this, and it is possible to reduce magnetic coupling between sets by adjusting the skew angle when designing a motor. In the healthy state, the coordinate transform method of ADTP-SM uses the Double dq transform and VSD model [7–12].

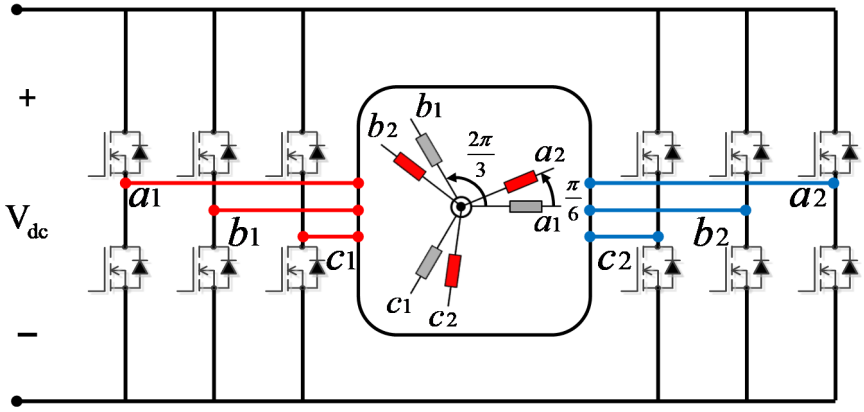


Figure 1. ADTP-SM drive system model [3,5].

Double dq transform performs the current control by selecting the *dq*-axis coordinate system for each set. The VSD model uses the *dq* axis for energy conversion and the *xy* axis for harmonic current control. The current projected on the *xy*-axis is controlled to zero [8–10,13,14].

In a single-phase open fault state, it can be controlled in the same way as a healthy situation. ADTP-SM can create a positive torque, due to the forward magneto motive force (MMF) component [15]. However, since both coordinate transformation methods do not have orthogonality between Cartesian coordinate systems, control stability is degraded. Double dq transform must control two *dq*-axes to generate a torque. On the other hand, the VSD model can control only the *dq*-axis to generate a torque, so it can be controlled stably even in the case of a single-phase open fault state [16–22].

This paper compares the current control characteristics of the Double dq transform and VSD model in healthy and single-phase open fault states. The harmonics projected on each reference frame are mathematically analyzed, and the current control characteristics are validated through simulations and experiments. Section 2 is a healthy state, and Section 3 is a single-phase open fault state. Section 4 summarizes the content as a conclusion.

2. Comparison of the Coordinate Transformation of ADTP-SM under Healthy Operation

The assumption of the following equation ignores the nonlinearity of the inverter, the saturation of the inductance, and the harmonic components of the inductance and flux linkage. The armature inductance is a 6 × 6 matrix. It is composed of a self-inductance of each phase, mutual inductance within the set, and mutual inductance between sets. To control ADTP-SM, coordinate transformation is applied to transform the time-varying term of the voltage equation into the time-invariant terms. Equation (1) is the phase voltage equation of ADTP-SM. The *v*, *i*, *R*, *L*, ψ, and *t* in the equation mean the voltage, current, resistance, inductance, field-linkage flux of each phase, and time. Subscripts *a*, *b*, *c* are phases and 1 and 2 are the number of sets. The diagonal components of the 6 × 6 inductance matrix are the self-inductance component, and the rest are the mutual-inductance component.

$$\begin{bmatrix} v_{a1} \\ v_{b1} \\ v_{c1} \\ v_{a2} \\ v_{b2} \\ v_{c2} \end{bmatrix} = \begin{bmatrix} i_{a1} \\ i_{b1} \\ i_{c1} \\ i_{a2} \\ i_{b2} \\ i_{c2} \end{bmatrix} \times R + \frac{\partial}{\partial t} \begin{bmatrix} L_{a1a1} & L_{a1b1} & L_{a1c1} & L_{a1a2} & L_{a1b2} & L_{a1c2} \\ & L_{b1b1} & L_{b1c1} & L_{b1a2} & L_{b1b2} & L_{b1c2} \\ & & L_{c1c1} & L_{c1a2} & L_{c1b2} & L_{c1c2} \\ & & & L_{a2a2} & L_{a2b2} & L_{a2c2} \\ & & & & L_{b2b2} & L_{b2c2} \\ sym & & & & & L_{c2c2} \end{bmatrix} \times \begin{bmatrix} i_{a1} \\ i_{b1} \\ i_{c1} \\ i_{a2} \\ i_{b2} \\ i_{c2} \end{bmatrix} + \frac{\partial}{\partial t} \begin{bmatrix} \psi_{a1} \\ \psi_{b1} \\ \psi_{c1} \\ \psi_{a2} \\ \psi_{b2} \\ \psi_{c2} \end{bmatrix} \quad (1)$$

2.1. Double dq Transformation under Healthy Operation

Double dq transform is a control method using the *dq*-axis coordinate systems of sets 1 and 2, respectively. Equation (1) can be converted by applying Equations (2)–(5). The f is an arbitrary variable of ADTP-SM, and s, e in the superscript mean the stationary coordinate system and the rotational coordinate system, respectively. Equations (4) and (5) are the rotational and the stationary coordinate transformation matrix of the Double dq transform.

$$f_{Double}{}^{e} = T_{Double}{}^{e} \times T_{Double}{}^{s} \times f_{abc} \tag{2}$$

$$\begin{bmatrix} f_{d1}{}^{e} & f_{q1}{}^{e} & f_{d2}{}^{e} & f_{q2}{}^{e} \end{bmatrix}^{T} = T_{Double}{}^{e} \times T_{Double}{}^{s} \times \begin{bmatrix} f_{a1} & f_{b1} & f_{c1} & f_{a2} & f_{b2} & f_{c2} \end{bmatrix}^{T} \tag{3}$$

$$T_{Double}{}^{e} = \begin{bmatrix} \cos(\theta) & \sin(\theta) & 0 & 0 \\ -\sin(\theta) & \cos(\theta) & 0 & 0 \\ 0 & 0 & \cos(\theta) & \sin(\theta) \\ 0 & 0 & -\sin(\theta) & \cos(\theta) \end{bmatrix} \tag{4}$$

$$T_{Double}{}^{s} = \frac{2}{3}\begin{bmatrix} \cos\left(-\frac{0\pi}{6}\right) & \cos\left(-\frac{4\pi}{6}\right) & \cos\left(-\frac{8\pi}{6}\right) & 0 & 0 & 0 \\ -\sin\left(-\frac{0\pi}{6}\right) & -\sin\left(-\frac{4\pi}{6}\right) & -\sin\left(-\frac{8\pi}{6}\right) & 0 & 0 & 0 \\ 0 & 0 & 0 & \cos\left(-\frac{1\pi}{6}\right) & \cos\left(-\frac{5\pi}{6}\right) & \cos\left(-\frac{9\pi}{6}\right) \\ 0 & 0 & 0 & -\sin\left(-\frac{1\pi}{6}\right) & -\sin\left(-\frac{5\pi}{6}\right) & -\sin\left(-\frac{9\pi}{6}\right) \end{bmatrix} \tag{5}$$

Equation (6) is the voltage equation to which the Double dq transform is applied. The θ is the electrical angle, ω is the electrical angular velocity, and the subscripts d and q are the *dq*-axes. Equation (7) is a torque equation consisting of the magnetic torque of sets 1 and 2, the reluctance torque of each set, and the reluctance torque due to mutual inductance between the sets. The L_{d1d1} and L_{q1q1} are the self-inductances of the d-axis and q-axis of set 1. The L_{d1d2} and L_{q1q2} are the mutual-inductances of the d-axis and q-axis of set 1 and 2. The L_{d2d2} and L_{q2q2} are the self-inductances of the d-axis and q-axis of set 2. The $\psi_{f1}{}^{e}$ and $\psi_{f2}{}^{e}$ are the field-linkage flux of sets 1 and 2. The pp is the number of pole pairs of the motor.

$$\begin{bmatrix} v_{d1}{}^{e} \\ v_{q1}{}^{e} \\ v_{d2}{}^{e} \\ v_{q2}{}^{e} \end{bmatrix} = R\begin{bmatrix} i_{d1}{}^{e} \\ i_{q1}{}^{e} \\ i_{d2}{}^{e} \\ i_{q2}{}^{e} \end{bmatrix} + \omega\begin{bmatrix} 0 & -L_{q1q1} & 0 & -L_{q1q2} \\ L_{d1d1} & 0 & L_{d1d2} & 0 \\ 0 & -L_{q1q2} & 0 & -L_{q2q2} \\ L_{d1d2} & 0 & L_{d2d2} & 0 \end{bmatrix} \times \begin{bmatrix} i_{d1}{}^{e} \\ i_{q1}{}^{e} \\ i_{d2}{}^{e} \\ i_{q2}{}^{e} \end{bmatrix} + \omega\begin{bmatrix} 0 \\ \psi_{f1}{}^{e} \\ 0 \\ \psi_{f2}{}^{e} \end{bmatrix} \tag{6}$$

$$Torque = pp \times \frac{3}{2}\left\{ \begin{array}{l} \psi_{f1}{}^{e} i_{q1}{}^{e} + \psi_{f2}{}^{e} i_{q2}{}^{e} + \\ \left(L_{d1d1} - L_{q1q1}\right) i_{d1}{}^{e} i_{q1}{}^{e} + \left(L_{d2d2} - L_{q2q2}\right) i_{d2}{}^{e} i_{q2}{}^{e} + \\ \left(L_{d2d1} - L_{q1q2}\right) i_{d1}{}^{e} i_{q2}{}^{e} + \left(L_{d1d2} - L_{q2q1}\right) i_{d2}{}^{e} i_{q1}{}^{e} \end{array} \right\} \tag{7}$$

The harmonic order projected on the *dq*-axis because of the Double dq transform can be obtained by Equation (8). The d-axis and the q-axis are orthogonal, and since set 1 and set 2 differ only in phase difference, the same harmonic order is projected. Assuming that the phase difference of f_{a1}, f_{b1}, and f_{c1} is 120 degrees and is an odd and cosine function, n is the odd harmonic order. If the θ is zero, it is the harmonic order projected onto the stationary coordinate system.

$$\begin{aligned} f_{d1}{}^{s} &= \begin{bmatrix} \cos\left(\theta - \frac{0\pi}{6}\right) & \cos\left(\theta - \frac{4\pi}{6}\right) & \cos\left(\theta - \frac{8\pi}{6}\right) \end{bmatrix} \times \begin{bmatrix} f_{a1} & f_{b1} & f_{c1} \end{bmatrix}^{T} \\ &= \sum_{n\,=\,odd} \frac{1}{2}\begin{bmatrix} \{\cos(1 \pm n)\theta\} \times \left\{\cos\left(\frac{(1\pm n)0\pi}{6}\right) + \cos\left(\frac{(1\pm n)4\pi}{6}\right) + \cos\left(\frac{(1\pm n)8\pi}{6}\right)\right\} + \\ \{\sin(1 \pm n)\theta\} \times \left\{\sin\left(\frac{(1\pm n)0\pi}{6}\right) + \sin\left(\frac{(1\pm n)4\pi}{6}\right) + \sin\left(\frac{(1\pm n)8\pi}{6}\right)\right\} \end{bmatrix} \end{aligned} \tag{8}$$

In Equation (8), if orthogonality is established, $f_{d1}{}^{s}$ becomes zero, otherwise, it has a value. When n becomes the 6k $\pm$ 1th (1st, 5th, 7th, 11th, 13th, ...) order component, the

$f_{d1}{}^{s}$ has a value other than zero. At this time, the harmonic components are projected onto the *dq*-axis of set 1 and 2. The block diagram of the Double dq transform current control is shown in Figure 2. The superscript * is the command value for the control. The same *dq*-axis reference currents are input to sets 1 and 2 and are controlled using a proportional and integral (PI) controller.

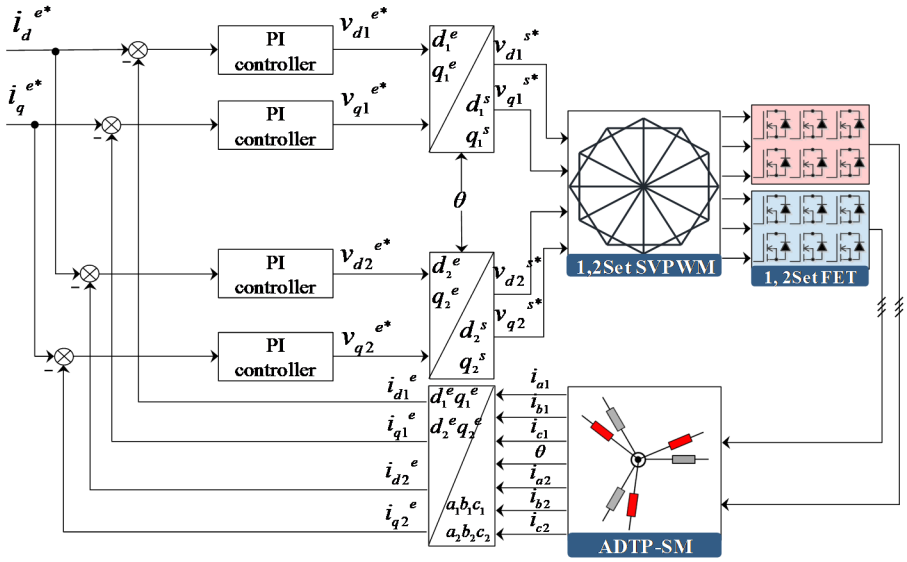


Figure 2. Current control block diagram applying Double dq transform of ADTP-SM.

2.2. VSD Model under Healthy Operation

The VSD model is applicable for ADTP-SM with a phase difference of 30 degrees between sets. This coordinate transformation method constitutes two coordinate systems. It consists of a *dq*-axis for energy conversion and a *xy*-axis for controlling current harmonics. Equation (1) can be converted into a VSD model by applying Equations (9) to (12). Equations (11) and (12) are the rotational coordinate transformation matrix and the stationary coordinate transformation matrix of the VSD model. There are two methods to converts the $x^e y^e$-axis. One method uses five times the electric angle and the other method uses the same electric angle as the *dq*-axis. In the former case, the 5th harmonics of the phase current are projected as DC components, and the remaining harmonics are projected as AC components.

$$f_{VSD}{}^{e} = T_{VSD}{}^{e} \times T_{VSD}{}^{s} \times f_{abc} \tag{9}$$

$$\begin{bmatrix} f_d{}^e & f_q{}^e & f_x{}^e & f_y{}^e \end{bmatrix}^T = T_{VSD}{}^{e} \times T_{VSD}{}^{s} \times \begin{bmatrix} f_{a1} & f_{b1} & f_{c1} & f_{a2} & f_{b2} & f_{c2} \end{bmatrix}^T \tag{10}$$

$$T_{VSD}{}^{e} = \begin{bmatrix} \cos(\theta) & \sin(\theta) & 0 & 0 \\ -\sin(\theta) & \cos(\theta) & 0 & 0 \\ 0 & 0 & \cos(\theta) & -\sin(\theta) \\ 0 & 0 & -\sin(\theta) & -\cos(\theta) \end{bmatrix} \tag{11}$$

$$T_{VSD}{}^{s} = \frac{1}{3}\begin{bmatrix} \cos\left(-\frac{0\pi}{6}\right) & \cos\left(-\frac{4\pi}{6}\right) & \cos\left(-\frac{8\pi}{6}\right) & \cos\left(-\frac{1\pi}{6}\right) & \cos\left(-\frac{5\pi}{6}\right) & \cos\left(-\frac{9\pi}{6}\right) \\ -\sin\left(-\frac{0\pi}{6}\right) & -\sin\left(-\frac{4\pi}{6}\right) & -\sin\left(-\frac{8\pi}{6}\right) & -\sin\left(-\frac{1\pi}{6}\right) & -\sin\left(-\frac{5\pi}{6}\right) & -\sin\left(-\frac{9\pi}{6}\right) \\ \cos 5\left(-\frac{0\pi}{6}\right) & \cos 5\left(-\frac{4\pi}{6}\right) & \cos 5\left(-\frac{8\pi}{6}\right) & \cos 5\left(-\frac{1\pi}{6}\right) & \cos 5\left(-\frac{5\pi}{6}\right) & \cos 5\left(-\frac{9\pi}{6}\right) \\ -\sin 5\left(-\frac{0\pi}{6}\right) & -\sin 5\left(-\frac{4\pi}{6}\right) & -\sin 5\left(-\frac{8\pi}{6}\right) & -\sin 5\left(-\frac{1\pi}{6}\right) & -\sin 5\left(-\frac{5\pi}{6}\right) & -\sin 5\left(-\frac{9\pi}{6}\right) \end{bmatrix} \tag{12}$$

This has a disadvantage that the gain value of the PI controller should increase as the fundamental frequency increases. However, applying the latter case is an AC component

with no DC offset, so there is no need to increase the gain value of the PI controller [10]. In this paper, the latter case was applied. Equation (13) is the voltage equation of the VSD model. Compared with Equation (6), there is no mutual interference between the two coordinate systems. Equation (14) is a torque equation consisting of a magnetic torque and reluctance torque.

$$\begin{bmatrix} {v_d}^e \\ {v_q}^e \\ {v_x}^e \\ {v_y}^e \end{bmatrix} = R \begin{bmatrix} {i_d}^e \\ {i_q}^e \\ {i_x}^e \\ {i_y}^e \end{bmatrix} + \omega \begin{bmatrix} -L_q \\ L_d \\ -L_y \\ L_x \end{bmatrix} \times \begin{bmatrix} {i_d}^e \\ {i_q}^e \\ {i_x}^e \\ {i_y}^e \end{bmatrix} + \omega \begin{bmatrix} 0 \\ {\psi_f}^e \\ 0 \\ 0 \end{bmatrix} \tag{13}$$

$$Torque = pp \times 3\left\{ {\psi_f}^e {i_q}^e + \left(L_d - L_q\right) {i_d}^e {i_q}^e \right\} \tag{14}$$

As a result of the VSD model, the harmonic orders projected on the $d^s q^s$ and $x^s y^s$-axes can be obtained from Equations (15) and (16). The d^s-axis does not have orthogonality when n is 12k ± 1th order (1st, 11th, 13th, . . .) and the x^s-axis does not have orthogonality when n is 12k ± 5th order (5th, 7th, 17th, 19th, . . .).

$$f_d{}^s = \sum_{n\,=\,odd} \frac{1}{2} \left[\begin{array}{l} \{\cos(1 \pm n)\theta\} \times \left\{ \begin{array}{l} \cos\left(\frac{(1\pm n)0\pi}{6}\right) + \cos\left(\frac{(1\pm n)4\pi}{6}\right) + \cos\left(\frac{(1\pm n)8\pi}{6}\right) + \\ \cos\left(\frac{(1\pm n)1\pi}{6}\right) + \cos\left(\frac{(1\pm n)5\pi}{6}\right) + \cos\left(\frac{(1\pm n)9\pi}{6}\right) \end{array} \right\} + \\ \{\sin(1 \pm n)\theta\} \times \left\{ \begin{array}{l} \sin\left(\frac{(1\pm n)0\pi}{6}\right) + \sin\left(\frac{(1\pm n)4\pi}{6}\right) + \sin\left(\frac{(1\pm n)8\pi}{6}\right) + \\ \sin\left(\frac{(1\pm n)1\pi}{6}\right) + \sin\left(\frac{(1\pm n)5\pi}{6}\right) + \sin\left(\frac{(1\pm n)9\pi}{6}\right) \end{array} \right\} \end{array} \right] \tag{15}$$

$$f_x{}^s = \sum_{n\,=\,odd} \frac{1}{2} \left[\begin{array}{l} \{\cos(5 \pm n)\theta\} \times \left\{ \begin{array}{l} \cos\left(\frac{(5\pm n)0\pi}{6}\right) + \cos\left(\frac{(5\pm n)4\pi}{6}\right) + \cos\left(\frac{(5\pm n)8\pi}{6}\right) + \\ \cos\left(\frac{(5\pm n)1\pi}{6}\right) + \cos\left(\frac{(5\pm n)5\pi}{6}\right) + \cos\left(\frac{(5\pm n)9\pi}{6}\right) \end{array} \right\} + \\ \{\sin(5 \pm n)\theta\} \times \left\{ \begin{array}{l} \sin\left(\frac{(5\pm n)0\pi}{6}\right) + \sin\left(\frac{(5\pm n)4\pi}{6}\right) + \sin\left(\frac{(5\pm n)8\pi}{6}\right) + \\ \sin\left(\frac{(5\pm n)1\pi}{6}\right) + \sin\left(\frac{(5\pm n)5\pi}{6}\right) + \sin\left(\frac{(5\pm n)9\pi}{6}\right) \end{array} \right\} \end{array} \right] \tag{16}$$

Since the harmonic orders projected on the d^s-axis and the x^s-axis are different, the two Cartesian coordinate systems are independent of each other and no mutual interference occurs. The current control block diagram of the VSD model is shown in Figure 3. The $d^e q^e$-axis is composed of a PI controller in the same way as the Double dq transform.

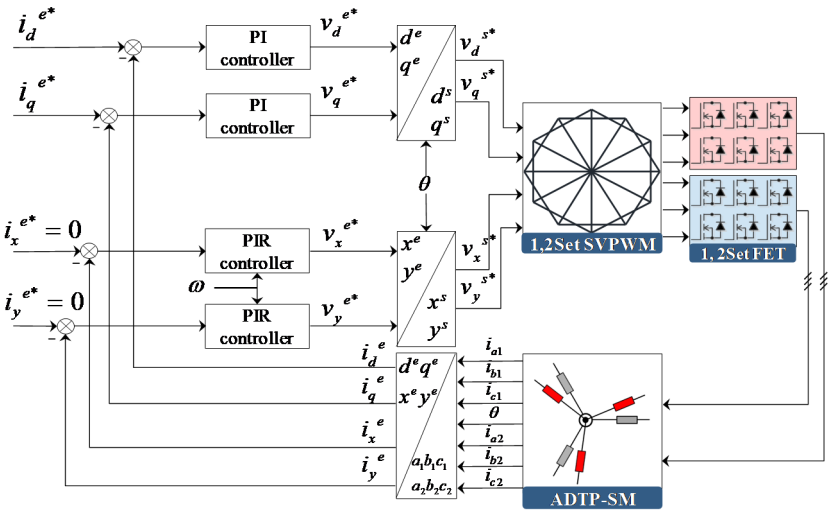


Figure 3. Current control block diagram applying the vector space decomposition (VSD) model of ADTP-SM.

The $x^e y^e$-axis is composed of a proportional, integral and resonance (PIR) controller by adding a resonance controller to control the projected AC component [13,14]. The

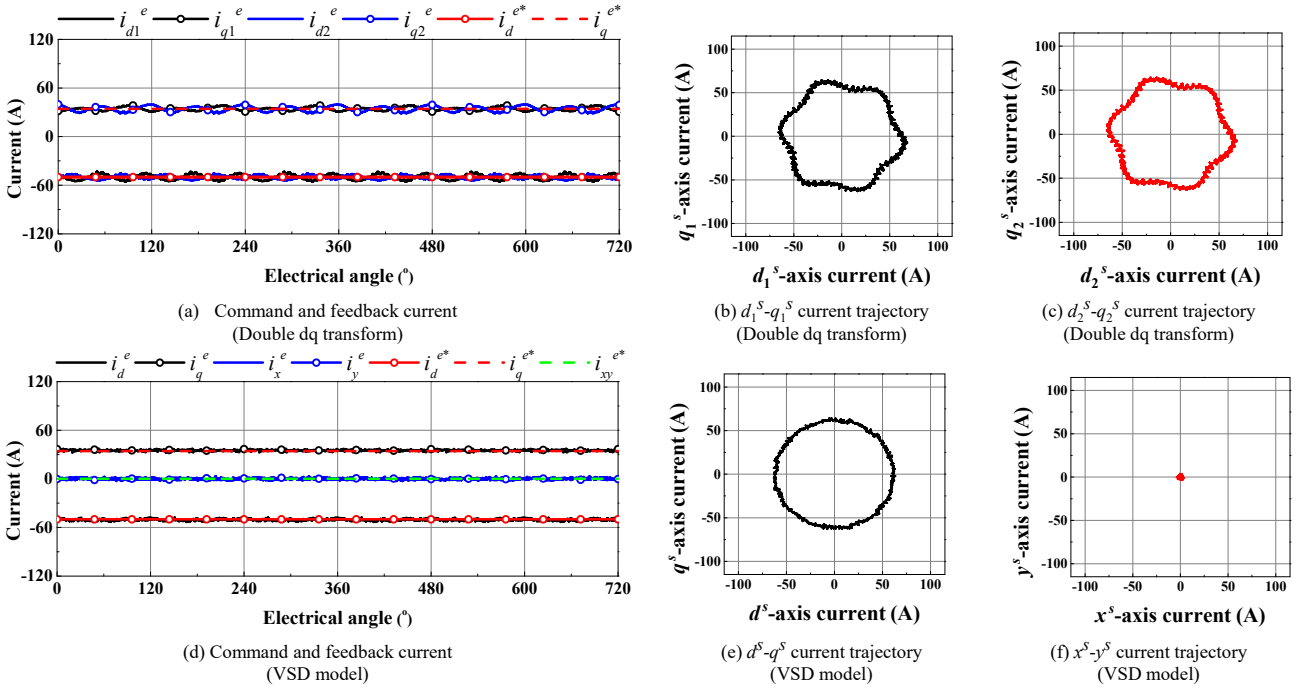
resonance frequency of the resonance controller is six times the fundamental frequency to control the 5th and 7th harmonics of the phase current.

2.3. Analysis of Simulation Results under Healthy Operation

The Matlab/Simulink was used to compare the control stability according to the coordinate transformation in a healthy operation [11,12]. The simulation conditions are as follows: the number of pole pairs = 8, the average value of the field-linkage flux = 14.33 mWb, R = 12.57 mΩ, the average value of the self-inductance is 0.05 mH, the rotating speed is 1000 rpm. The current command of the Double dq transform and VSD model is $i_d{}^{e*} = -50$ A, $i_q{}^{e*} = 34.2$ A.

As shown in Figure 4a,d, the oscillation of the feedback current in the d^eq^e-axis of the VSD model is small and the tracking performance for the command current is better. Therefore, stable current control is possible. When Double dq transform is applied, the current in the d^sq^s-axis contains the 5th and 7th harmonics, so the current trajectory is not circular. On the other hand, in the case of the VSD model, the 11th and 13th harmonics are projected on the d^sq^s-axis, and the size of the harmonic current is small, and it is circular. And since the x^ey^e-axis controls the projection current to 0, the size of the circle is very small. As shown in Figure 5, compared to the VSD model, when the Double dq transform is applied, many 5th and 7th harmonics are projected onto the phase current. On the other hand, the VSD model reduces harmonics by controlling the xy-axis. The total harmonic distortion (THD) of the $a1$ phase current is 9.90% when Double dq transform is applied and 2.46% when VSD model is applied.

Figure 6 is the torque profile. The black line is applied with Double dq transform and the red line is applied with a VSD model. The average torque is the same for both the black line and the red line, but the torque ripple is 2.81% when the Double dq transform is applied and 0.73% when the VSD model is applied. As a result of the simulation, the VSD model is a more stable control method when considering the stability of the feedback current for the command current, the THD of the phase current, and the torque profile.



(a) Command and feedback current (Double dq transform)
(b) $d_1{}^S$-$q_1{}^S$ current trajectory (Double dq transform)
(c) $d_2{}^S$-$q_2{}^S$ current trajectory (Double dq transform)
(d) Command and feedback current (VSD model)
(e) d^S-q^S current trajectory (VSD model)
(f) x^S-y^S current trajectory (VSD model)

Figure 4. Simulation results of rotational coordinate command, feedback currents (**a**,**d**) and stational coordinate current trajectory (**b**,**c**,**e**,**f**) when applying to the Double dq transform and VSD model.

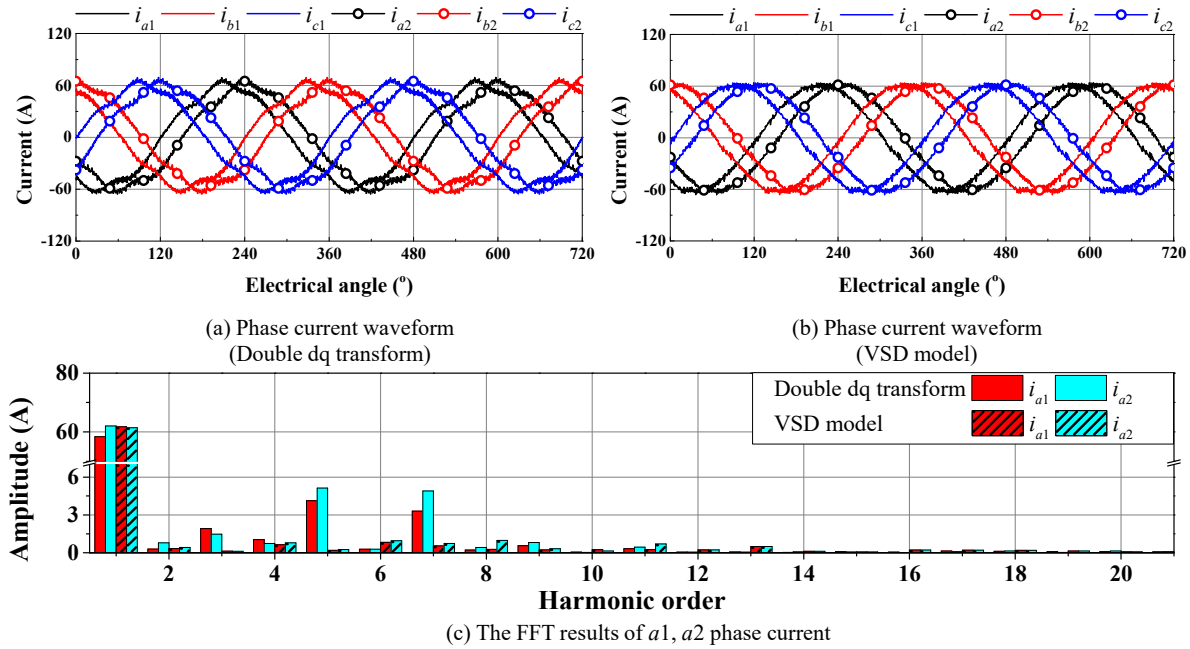


Figure 5. Simulation results of phase current waveform (**a**,**b**), and FFT analysis (**c**) when applying to the Double dq transform and VSD model.

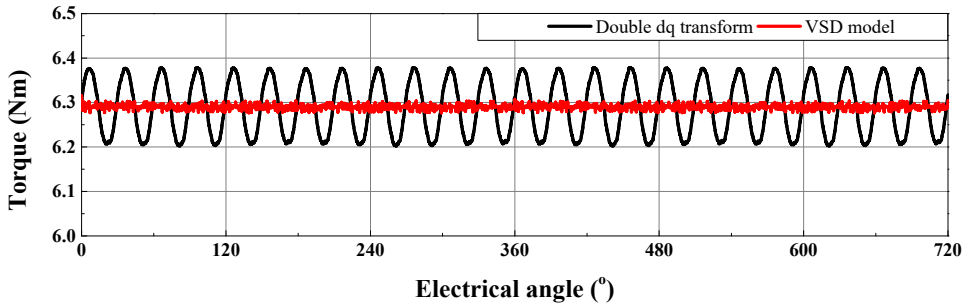


Figure 6. Torque profile of simulation results according to coordinate transformation method in healthy operation.

2.4. Analysis of Experiment Results under Healthy Operation

The experimental environment is shown in Figure 7. The input power of ADTP-SM uses a two-level voltage source inverter. The digital signal processor (DSP) uses MPC5744P of NXP Semiconductors and controls ADTP-SM using 12 pulse width modulation (PWM) signals. The experimental conditions are as follows: the number of pole pairs = 8, the average value of the field-linkage flux = 14.33 mWb, R = 12.57 mΩ, the average value of the self-inductance is 0.05 mH, the rotating speed is 1000 rpm. The current command is the same as the simulation condition. The sampling of the torque sensor is very low at 10 samples per second and the torque sensor is measured by the combined torque ripple of the dynamometer and ADTP-SM. Therefore, the torque ripple of only ADTP-SM cannot be measured, but the average torque can be measured. The experimental results are consistent with the simulation results, and the details are as follows.

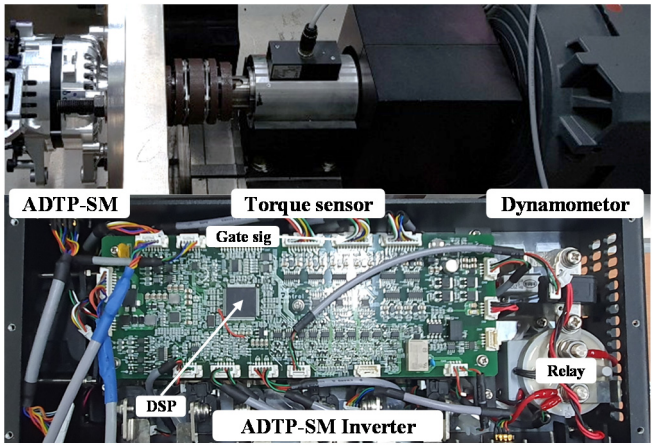
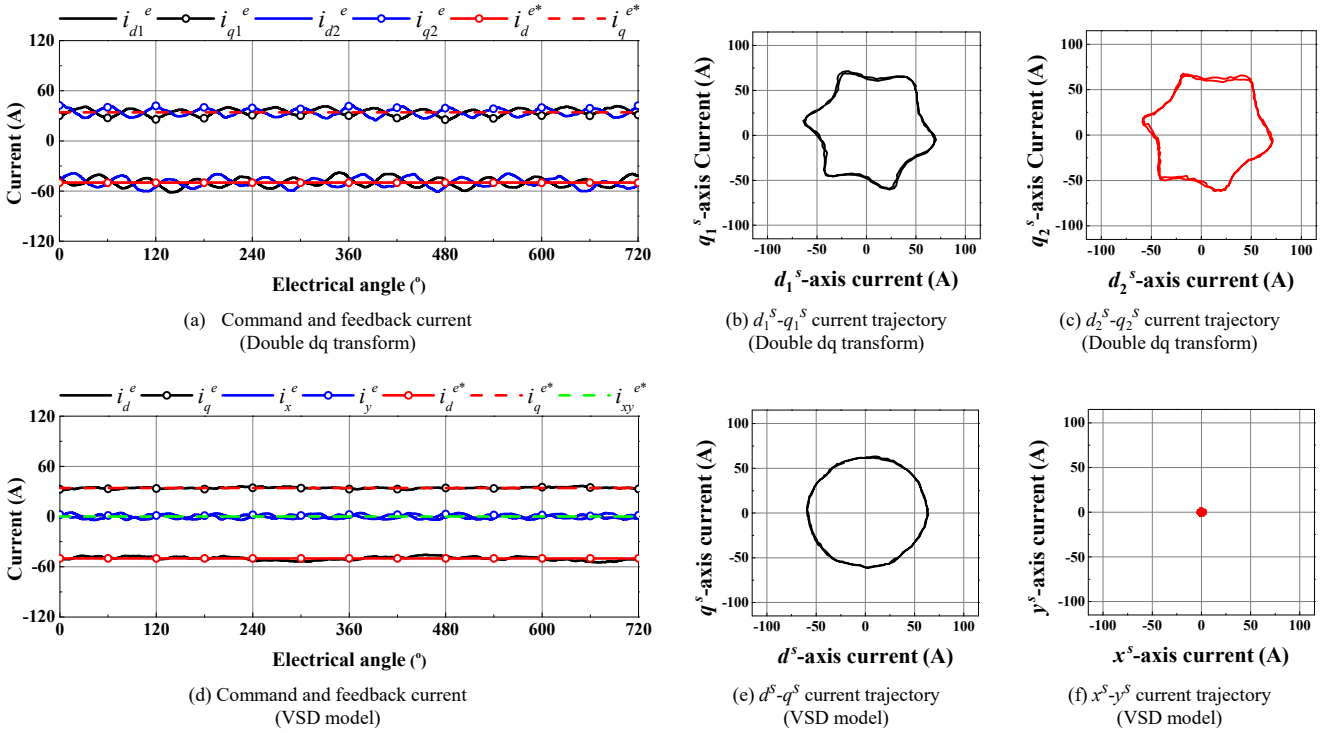


Figure 7. Picture of the experimental setup.

As shown in Figure 8, the stability of the feedback current for the command current is better in the VSD model. The current trajectory of the stationary coordinate system, and the Double dq transform, contains many harmonics compared to the VSD model. Since many harmonics are included in the stationary coordinate system current trajectory of the Double dq transform, the trajectory is not circular, whereas the current trajectory of the VSD model is circular. Furthermore, the current trajectory of the $x^s y^s$-axis of the VSD model and the projected harmonic current is controlled to zero.



(a) Command and feedback current (Double dq transform)

(b) d_1^s-q_1^s current trajectory (Double dq transform)

(c) d_2^s-q_2^s current trajectory (Double dq transform)

(d) Command and feedback current (VSD model)

(e) d^s-q^s current trajectory (VSD model)

(f) x^s-y^s current trajectory (VSD model)

Figure 8. Experiment results of rotational coordinate command, feedback currents (**a**,**d**), and stational coordinate current trajectory (**b**,**c**,**e**,**f**) when applying to the Double dq transform and VSD model.

Figure 9a,b is the phase current waveforms, and Figure 9c shows the FFT analysis results of the *a*1 and *a*2 phases currents. When the VSD model is applied, the $x^e y^e$-axis controls the harmonic current to zero, so it is a more sinusoidal phase current waveform. The THD of the *a*1 phase current is 12.12% when the Double dq transform is applied and 6.66% when the VSD model is applied.

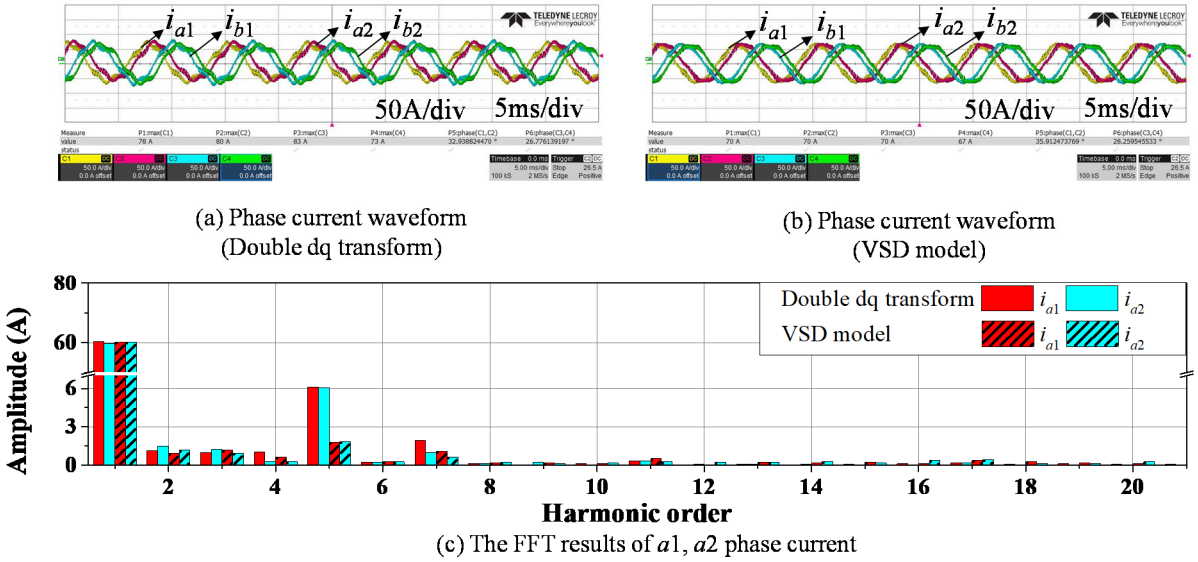


Figure 9. (**a**–**c**) Experiment results of phase current profile, and FFT analysis when applying to the Double dq transform and VSD model.

Figure 10 is the torque profile, and the average torque is the same. The torque ripple is 0.71% for VSD model and 1.75% for double dq transform.

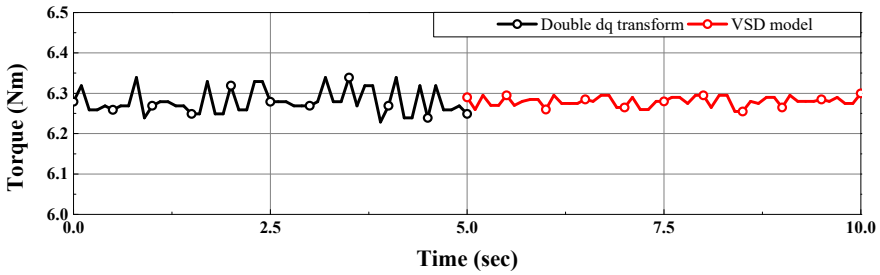


Figure 10. Torque profile of experimental results according to coordinate transformation method in healthy operation.

As with the simulation results, the experimental results have better control characteristics and stability when applying the VSD model. Furthermore, since it has a low THD and low torque ripple, it is reasonable to apply the VSD model in a healthy operation.

3. Comparison of the Coordinate Transformation of ADTP-SM under Single-Phase Open Fault

This Section compares the control stability according to the transform method when the c_2 phase is in a single-phase open fault. As in Section 2, when applying the Double dq transform and VSD model, the experimental results are analyzed.

3.1. Double dq Transform under Single-Phase Open Fault

In a postfault operation, the current of the two-phases of the fault set has the same magnitude and opposite sign. The current of the fault phase (c_2) is zero. When Equations (2)–(5) are applied, the same magnitude as the phase current of the fault set cannot be generated.

Furthermore, it is not possible to maintain a phase difference of 30 degrees between sets. Equation (17) is the stationary and rotational coordinate system current for the fault set.

$$\begin{array}{rcl} {f_{d2}}^s & = & \frac{2}{3} \times \left\{ \frac{\sqrt{3}}{2} f_{a2} - \frac{\sqrt{3}}{2} f_{b2} \right\} \; = \; \frac{2}{\sqrt{3}} \times f_{a2} \\ {f_{q2}}^s & = & \frac{2}{3} \times \left\{ \frac{1}{2} f_{a2} + \frac{1}{2} f_{b2} \right\} \; = \; 0 \\ {f_{d2}}^e & = & \frac{2}{\sqrt{3}} f_{a2} \cos\theta \\ {f_{q2}}^e & = & -\frac{2}{\sqrt{3}} f_{a2} \sin\theta \end{array} \tag{17}$$

As shown in Equation (18), if the phase current on a_2 is a cosine function, the current projected on the rotational coordinate system fluctuates at twice in one periodic of electrical angle. Due to mutual inductance, the d_1q_1 and d_2q_2-axes interfere with each other.

$$\begin{array}{rcl} {f_{d2}}^e & = & \frac{1}{\sqrt{3}} (\cos 2\theta + 1) \\ {f_{q2}}^e & = & -\frac{1}{\sqrt{3}} \sin 2\theta \end{array} \tag{18}$$

3.2. VSD Model under Single-Phase Open Fault

Equation (19) is the stationary coordinate system variable of the dq and xy-axes in a fault situation [17,18,22]. The variable of q^s and y^s-axis is the same magnitude and opposite sign. Therefore, the d^sq^s and x^sy^s-axes are no longer orthogonal and cause mutual interference. Furthermore, the x^ey^e-axis does not reduce the harmonics of the phase current and deteriorates the control stability of ADTP-SM. When controlling using only the d^eq^e-axis, control stability can be improved because there is no Cartesian coordinate system other than the d^eq^e-axis. Equation (20) is a transformation from a rotational coordinate system to a phase variable when only the dq-axis is considered. Equation (21) is an expansion of Equation (20), and the value of the specific phase is $\frac{\sqrt{13}}{2}$ times greater than the value of the rotational coordinate system variable [18]. The phases in the healthy set are also unbalanced and the phase difference is not 120°.

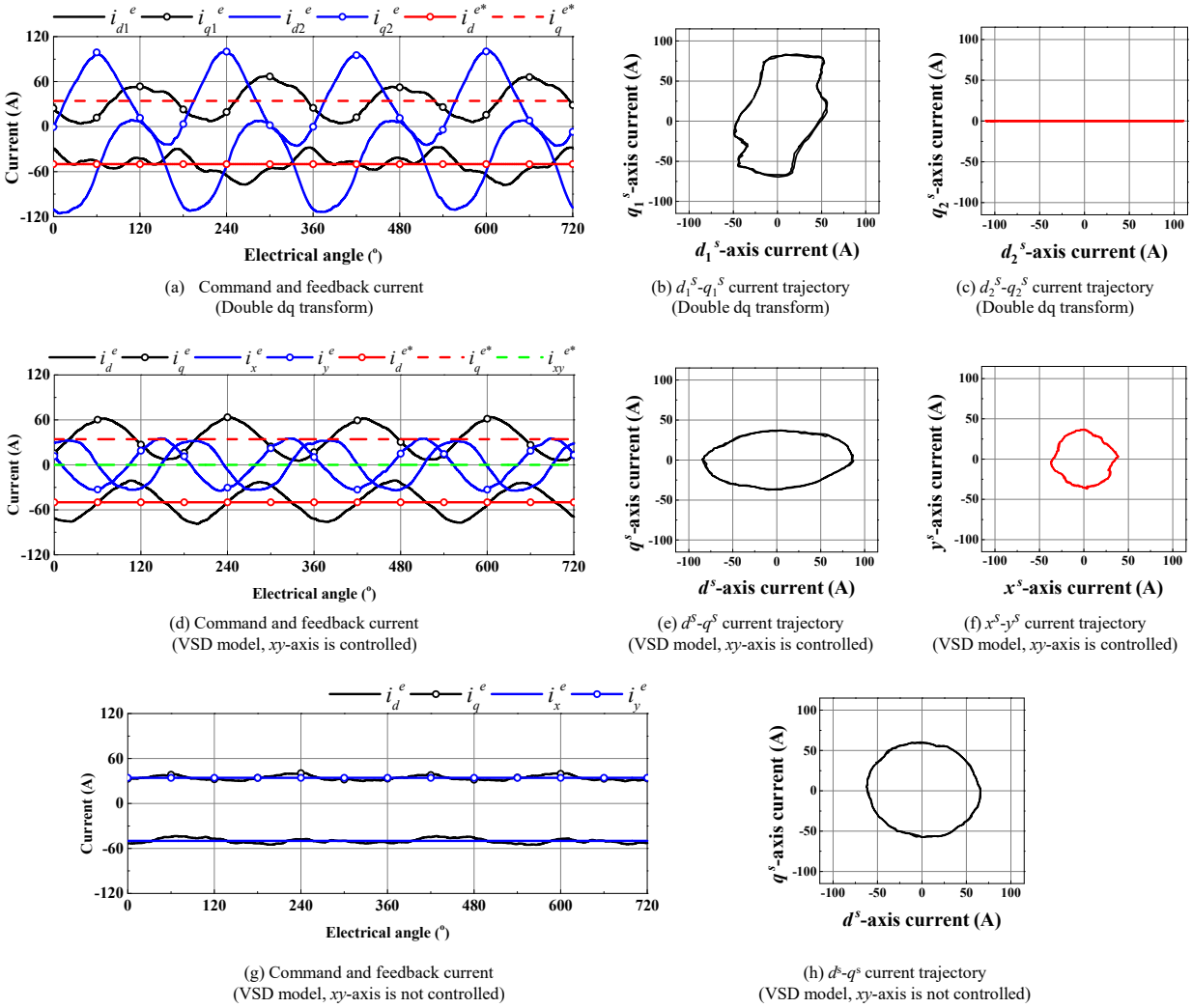
$$\begin{array}{rcl} {f_d}^s & = & \frac{1}{3} \times \left(f_{a1} - \frac{1}{2} f_{b1} - \frac{1}{2} f_{c1} + \sqrt{3} f_{a2} \right) \\ {f_q}^s & = & \frac{1}{3} \times \left(\frac{\sqrt{3}}{2} f_{a1} - \frac{\sqrt{3}}{2} f_{c1} \right) \\ {f_x}^s & = & \frac{1}{3} \times \left(f_{a1} - \frac{1}{2} f_{b1} - \frac{1}{2} f_{c1} - \sqrt{3} f_{a2} \right) \\ {f_y}^s & = & \frac{1}{3} \times \left(-\frac{\sqrt{3}}{2} f_{b1} + \frac{\sqrt{3}}{2} f_{c1} \right) \end{array} \tag{19}$$

$$\begin{bmatrix} f_{a1} & f_{b1} & f_{c1} & f_{a2} & f_{b2} & f_{c2} \end{bmatrix}^T = \begin{bmatrix} 1 & -\frac{1}{2} & -\frac{1}{2} & \frac{\sqrt{3}}{2} & -\frac{\sqrt{3}}{2} \\ 0 & \sqrt{3} & -\sqrt{3} & 0 & 0 \end{bmatrix}^T \times \begin{bmatrix} \cos\theta & -\sin\theta \\ \sin\theta & \cos\theta \end{bmatrix} \times \begin{bmatrix} {f_d}^e & {f_q}^e \end{bmatrix}^T \tag{20}$$

$$\begin{bmatrix} f_{a1} \\ f_{b1} \\ f_{c1} \\ f_{a2} \\ f_{b2} \end{bmatrix} = \begin{bmatrix} \cos\theta & -\sin\theta \\ \frac{\sqrt{13}}{2}\cos(\theta - 0.589\pi) & -\frac{\sqrt{13}}{2}\sin(\theta - 0.589\pi) \\ \frac{\sqrt{13}}{2}\cos(\theta + 0.589\pi) & -\frac{\sqrt{13}}{2}\sin(\theta + 0.589\pi) \\ \frac{\sqrt{3}}{2}\cos\theta & -\frac{\sqrt{3}}{2}\sin\theta \\ -\frac{\sqrt{3}}{2}\cos\theta & \frac{\sqrt{3}}{2}\sin\theta \end{bmatrix} \times \begin{bmatrix} {f_d}^e \\ {f_q}^e \end{bmatrix} \tag{21}$$

3.3. Analysis of Experiment Results under Single-Phase Open Fault

The experimental environment and conditions are as in Section 2.4. Figure 11a–c shows the results of when the Double dq transform is applied. When applying the VSD model, the results of controlling both the d^eq^e and x^ey^e-axes are seen in Figure 11d–f, and the result of controlling only the d^eq^e-axis is Figure 11g,h. Figure 11a is the feedback current for the command current, and as shown in Equation (18), the feedback current of the fault set fluctuates.



(a) Command and feedback current (Double dq transform)

(b) d_1^S-q_1^S current trajectory (Double dq transform)

(c) d_2^S-q_2^S current trajectory (Double dq transform)

(d) Command and feedback current (VSD model, xy-axis is controlled)

(e) d^S-q^S current trajectory (VSD model, xy-axis is controlled)

(f) x^S-y^S current trajectory (VSD model, xy-axis is controlled)

(g) Command and feedback current (VSD model, xy-axis is not controlled)

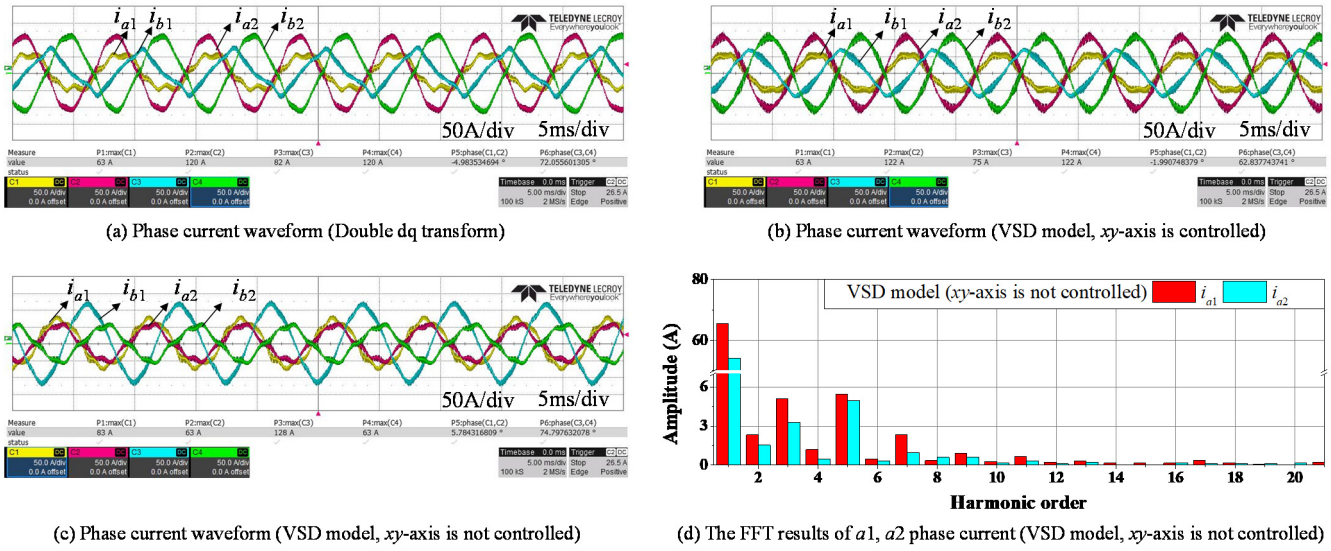
(h) d^s-q^s current trajectory (VSD model, xy-axis is not controlled)

Figure 11. (**a**–**h**) Experiment results of rotational coordinate command, feedback currents, and stational coordinate current trajectory when applying to the Double dq transform and VSD model (current waveform when xy-axis is controlled and when not controlled).

It is difficult to control stably, due to mutual interference between the d_1q_1 and d_2q_2-axes. As a result, the current trajectory of the stationary coordinate system of set 1, as shown in Figure 11b, is not circular. Figure 11c is the current trajectory of the stationary coordinate system of set 2, and the $i_{q2}{}^s$ current is 0, as shown in Equation (17). Figure 11d is the feedback current for the current command when both the d^eq^e and x^ey^e-axes are controlled. As can be seen from Equation (19), it is difficult to control stably because orthogonality between the q^s and y^s-axes is not established. Figure 11e,f are the current trajectories d^sq^s and x^sy^s-axes of the VSD model. The current trajectory on the d^sq^s-axis is not circular. Figure 11g is the feedback current for the command current when only d^eq^e-axis is controlled, and (h) is the d^sq^s-axis current trajectory. As mentioned in Section 3.2, since only the d^eq^e-axis is controlled, it can be controlled stably, and the current trajectory is also circular.

Figure 12a is the phase current waveform when the Double dq transform is applied. When applying the VSD model, the current waveform controlled by both the d^eq^e and x^ey^e-axes is shown in Figure 12b, and the current waveform that controlled only the d^eq^e-axis is shown in Figure 12c. Figure 12a,b is the current waveforms when mutual interference occurs between different Cartesian coordinate systems (d_1q_1 and d_2q_2-axes, dq and xy-axes) during current control. These are currents determined by the influence of a specific speed and PI controller gain, so it is difficult to analyze mathematically (FFT analysis). The

current waveform in Figure 12c can be analyzed by Equation (21), and the experimental current error is about 7.95% for i_{a1} and 2.94% for i_{a2} based on the fundamental frequency. THD is 12.88% for i_{a1} and higher than during the healthy operation with i_{a2} = 11.74%. Figure 13 is a torque profile, and it has the lowest torque ripple value when the $x^e y^e$-axis is not controlled when the VSD model is applied. All three coordinate transformation methods output a similar average torque, but this may vary depending on the conditions and magnitude of the command.



(a) Phase current waveform (Double dq transform)

(b) Phase current waveform (VSD model, *xy*-axis is controlled)

(c) Phase current waveform (VSD model, *xy*-axis is not controlled)

(d) The FFT results of *a*1, *a*2 phase current (VSD model, *xy*-axis is not controlled)

Figure 12. (**a**–**d**) Experiment results of phase current waveform according to the coordinate transformation methods in a single-phase open fault.

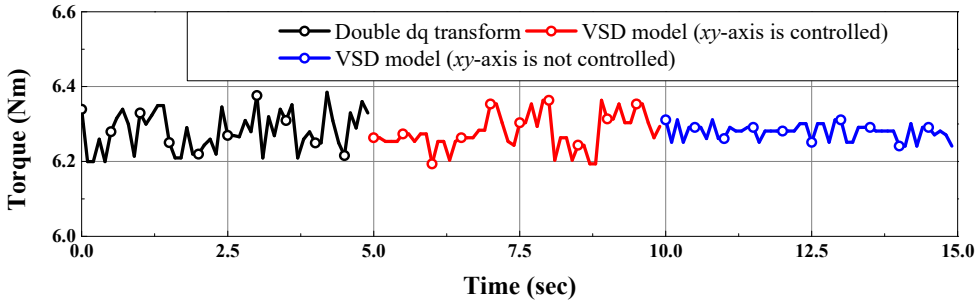


Figure 13. Torque profile of experimental results according to the coordinate transformation method in a single-phase open fault.

4. Conclusions

Coordinate transformation methods for controlling the current of ADTP-SM are the Double dq transform and VSD model. The control characteristics of the two methods are compared in healthy and single-phase open fault states. In the healthy state, current control is possible in both methods. However, when the VSD model is applied compared to the Double dq transform, the control stability of the feedback current for the command current is excellent, and the THD of the phase current can be improved. In the single-phase open fault state, if the Double dq transform and the $x^e y^e$-axis of the VSD model are controlled to 0, stable control is impossible. However, when only the $d^e q^e$-axis of the VSD model is controlled, there is no mutual interference between other Cartesian coordinate systems, so it can be controlled stably. This result was verified through mathematical methods, simulations, and experiments.

Author Contributions: Conceptualization, D.-K.S.; methodology, D.-K.S.; software, D.-K.S. and S.-H.K.; validation, D.-O.K., H.-S.S.; formal analysis, D.-K.S.; investigation, D.-O.K.; resources, D.-K.S.; data curation, S.-H.K.; writing—original draft preparation, D.-K.S.; writing—review and editing, S.-H.K. and D.-O.K.; visualization, D.-K.S.; supervision, G.-H.L. All authors have read and agreed to the published version of the manuscript.

Funding: This work was partly supported by the National Research Foundation of Korea (NRF) grant funded by the Korea government (MSIT) (Innovative Incubation Center for Autonomous xEV Technology) (No. 5199990814084). This work was also supported by the Korea Evaluation Institute of Industrial Technology (KEIT) (No. 20011866).

Institutional Review Board Statement: Not applicable.

Informed Consent Statement: Not applicable.

Data Availability Statement: Not applicable.

Conflicts of Interest: The authors declare no conflict of interest.

References

1. Parsa, L. On advantages of multi-phase machines. In Proceedings of the 31st Annual Conference of IEEE Industrial Electronics Society, 2005, IECON 2005, Raleigh, NC, USA, 6–10 November 2005; IEEE: Piscataway, NJ, USA, 2005; p. 6.
2. Levi, E. Advances in converter control and innovative exploitation of additional degrees of freedom for multiphase machines. *IEEE Trans. Ind. Electron.* **2016**, *63*, 433–448. [CrossRef]
3. Levi, E. Multiphase Electric Machines for Variable-Speed Applications. *IEEE Trans. Ind. Electron.* **2008**, *55*, 1893–1909. [CrossRef]
4. Miller, T.; McGilp, M. Analysis of multi-phase permanent-magnet synchronous machines. In Proceedings of the 2009 International Conference on Electrical Machines and Systems, Tokyo, Japan, 15–18 November 2009; pp. 1–6.
5. Gopakumar, K.; Ranganathan, V.T.; Bhat, S.R. Split-phase induction motor operation from PWM voltage source inverter. *IEEE Trans. Ind. Appl.* **1993**, *29*, 927–932. [CrossRef]
6. Karttunen, J.; Kallio, S.; Peltoniemi, P.; Silventoinen, P.; Pyrhonen, O. Dual three-phase permanent magnet synchronous machine supplied by two independent voltage source inverters. In Proceedings of the International Symposium on Power Electronics Power Electronics, Electrical Drives, Automation and Motion, Sorrento, Italy, 20–22 June 2012; pp. 741–747. [CrossRef]
7. Knudsen, H. Extended Park's transformation for 2x3-phase synchronous machine and converter phasor model with representation of AC harmonics. *IEEE Trans. Energy Convers.* **1995**, *10*, 126–132. [CrossRef]
8. Hu, Y.; Zhu, Z.Q.; Odavic, M. Comparison of Two-Individual Current Control and Vector Space Decomposition Control for Dual Three-Phase PMSM. *IEEE Trans. Ind. Appl.* **2017**, *53*, 4483–4492. [CrossRef]
9. Zhao, Y.; Lipo, T.A. Space Vector PWM Control of Dual Three-Phase Induction Machine Using Vector Space De-composition. *IEEE Trans. Ind. Appl.* **1995**, *31*, 1100–1109. [CrossRef]
10. Ruan, Z.; Song, W.; Yan, Y. Current Harmonic Suppression for Dual Three-Phase Permanent Magnet Synchronous Motor Drives. *IEEE Access* **2019**, *7*, 143888–143898. [CrossRef]
11. Arnold, R.; Haerri, V.V. Modelling and field orientated current control of a two-star 6-phase IPMSM for gearless wheel drives. In Proceedings of the 2011 IEEE International Electric Machines & Drives Conference (IEMDC), Niagara Falls, ON, Canada, 14–17 May 2011; pp. 539–544. [CrossRef]
12. James, A.E.; Anih, L.; Okoro, O. Transient Analysis and Modelling of Sixphase Asynchronous Machine. *Am. J. Electr. Power Energy Syst.* **2015**, *4*, 77. [CrossRef]
13. Karimi-Ghartemani, M.; Khajehoddin, S.A.; Mojiri, M.; Jain, P.; Bakhshai, A. A resonant controller with robust features for digital implementations at low sampling frequency. In Proceedings of the IECON 2012–38th Annual Conference on IEEE Industrial Electronics Society, Montreal, QC, Canada, 25–28 October 2012; Volume 27, pp. 5910–5915. [CrossRef]
14. Liserre, M.; Teodorescu, R.; Blaabjerg, F. Multiple harmonics control for three-phase grid converter systems with the use of PI-RES current controller in a rotating frame. *IEEE Trans. Power Electron.* **2006**, *21*, 836–841. [CrossRef]
15. Fu, J.; Lipo, T.A. Disturbance-Free Operation of a Multiphase Current-Regulated Motor Drive with an Opened Phase. *IEEE Trans. Ind. Appl.* **1994**, *30*, 1267–1274.
16. Ting, D.; Fenghui, L.; Li, S. Fault-tolerant method for six-phase PMSM by adjusting phase angle. In Proceedings of the 2017 20th International Conference on Electrical Machines and Systems (ICEMS), Sydney, Australia, 11–14 August 2017; pp. 1–5. [CrossRef]
17. Feng, G.; Lai, C.; Li, W.; Tjong, J.; Kar, N.C. Open-Phase Fault Modeling and Optimized Fault-Tolerant Control of Dual Three-Phase Permanent Magnet Synchronous Machines. *IEEE Trans. Power Electron.* **2019**, *34*, 11116–11127. [CrossRef]
18. Ryu, H.-M.; Kim, J.-W.; Sul, S.-K. Synchronous frame current control of multi-phase synchronous motor part II. asymmetric fault condition due to open phases. In Proceedings of the Conference Record of the 2004 IEEE Industry Applications Conference, 2004. 39th IAS Annual Meeting, Seattle, WA, USA, 3–7 October 2004; Volume 1, pp. 268–275.
19. Zhou, C.; Tang, W.; Sun, X.D.; Zhou, Z.; Yang, G.; Su, J. Control strategy for dual three-phase PMSM based on reduced order mathematical model under fault condition due to open phases. *J. Eng.* **2018**, *2018*, 489–494. [CrossRef]

20. Zhang, W.; Xu, Y.; Chen, B. Control of Dual Three-Phase Permanent Magnet Synchronous Motor under Open Phase Fault Conditions. In Proceedings of the 2016 IEEE Vehicle Power and Propulsion Conference (VPPC), Hangzhou, China, 17–20 October 2016; IEEE: Piscataway, NJ, USA, 2016; pp. 1–5.
21. Wu, F.; Zheng, P.; Jahns, T.M. Six-phase fault-tolerant permanent magnet motor drives with reduced switch counts: Topology comparisons and hardware demonstration. In Proceedings of the 2015 IEEE Transportation Electrification Conference and Expo (ITEC), Dearborn, MI, USA, 14–17 June 2015; Institute of Electrical and Electronics Engineers (IEEE): Piscataway, NJ, USA, 2015; pp. 1–6.
22. Zheng, J.; Huang, S.; Rong, F.; Lye, M. Six-Phase Space Vector PWM under Stator One-Phase Open-Circuit Fault Condition. *Energies* **2018**, *11*, 1796. [CrossRef]